Arthritis Research & Therapy

RESEARCH

Open Access

The TLR-M-CSF axis is implicated in increased bone turnover and curve progression in adolescent idiopathic scoliosis

Kai Sheng[1,2], Daniel G. Bisson[1,2], Neil Saran[1], Jake Bourdages[1], Christopher Coluni[1], Kirby Upshaw[1,3], Kerstin Tiedemann[1], Svetlana V. Komarova[4], Jean A. Ouellet[1] and Lisbet Haglund[1,2*]

Abstract

Background Facet joint osteoarthritis (OA) is prevalent in patients with adolescent idiopathic scoliosis (AIS). The most pronounced OA presents above and below the curve's apex where the intervertebral rotation is the greatest. This indicates that facet joint OA is implicated and potentially contributes to AIS progression. OA impacts both cartilage and bone and we have previously demonstrated an association between lower bone quality and more severe OA in AIS facet joints. This study aimed to further investigate the molecular mechanisms underlying cartilage–bone crosstalk in the facet joints of patients with AIS.

Methods Unbiased deep RNA sequencing was performed to compare gene expression in facet joint chondrocytes of age-matched AIS patients and non-scoliotic individuals. Differentially expressed genes of interest were validated through qPCR and ELISA in a larger sample cohort. Key regulatory pathways involved in cartilage–bone crosstalk were identified through bioinformatic analysis. Functional studies were conducted by treating chondrocytes with TLR2 and TLR4 agonists, collecting conditioned media, and administering it to an in vitro osteoclastogenesis model. The expression of M-CSF, a key regulatory factor influencing osteoclast proliferation, was measured in individual facet joint cartilage samples at different spinal levels and correlated with cartilage morphological grade and 3D structural parameters extracted from spine reconstruction.

Results One thousand four hundred twenty six upregulated genes were detected, and gene ontology analysis revealed a significant enrichment of the TLR pathway, and bone-regulating biological processes in AIS chondrocytes. TLR activation of AIS chondrocytes induced expression of bone-regulating factors, including M-CSF, a key regulator of osteoclast proliferation. Furthermore, secreted factors from AIS chondrocytes enhanced osteoclast proliferation and maturation, with a stronger effect observed following TLR pre-activation. Clinically, M-CSF expression was found to correlate strongly with increased OA severity and a greater degree of intervertebral axial rotation.

Conclusions Together, our findings suggest that the TLR-M-CSF axis is implicated in osteoclastogenesis, resulting in increased bone turnover and may contribute to curve progression in AIS patients.

Keywords Scoliosis, Facet joints, Osteoarthritis, Subchondral bone, Osteoclast, Crosstalk

*Correspondence:
Lisbet Haglund
lisbet.haglund@mcgill.ca
Full list of author information is available at the end of the article

Introduction

Adolescent Idiopathic Scoliosis (AIS) impacts 2–5% of adolescents globally. It is characterized by a three-dimensional spine deformity and results in pain and reduced quality of life in many patients [1]. A lack of spinal stability may predispose individuals to the initiation of the deformity, with progression being driven by unbalanced forces in an increasingly asymmetrical spine [2, 3]. Although several genetic and phenotypic risk factors have been identified, they can explain only a portion of the cases [4–6]. Regardless of the origin, the progression of the disease is largely driven by a vicious cycle, where asymmetric forces lead to asymmetric growth modulation. Current treatment involves bracing, to slow down or prevent progression of the deformity. Despite this, about a quarter of patients progress and need invasive surgery to correct the deformity [7]. There are currently no effective disease-modifying drugs, in part due to our limited understanding of the idiopathic nature. In-depth clinical and experimental research is needed to understand the dynamic changes influencing growth modulation in the scoliotic spine.

Spine stability relies on a complex interplay of the vertebral bodies, facet joints, intervertebral discs, ligaments, tendons, and paraspinal muscles [8]. Degenerative changes in any of the tissues can disrupt the interplay and potentially contribute to the progression of AIS. Facet joints, situated bilaterally at the back of each vertebra, are critical in restricting axial rotation, and they absorb approximately 20% of the compressive loads placed on the spinal column [9]. Abnormal spinal curvature in adult degenerative scoliosis leads to unbalanced loads, resulting in cartilage degeneration [9, 10]. Adults with lumbar facet joint osteoarthritis (OA) exhibit thinner and more porous subchondral cortical plates and increased trabecular number [11–13]. We previously reported that patients with AIS present with severe facet joint OA, with a correlation between cartilage degeneration and reduced subchondral bone quality, primarily in the thoracic facet joints [14]. Interestingly, the most pronounced OA is found in facet joints above and below the apex where intervertebral rotation is evident. [14, 15]. In contrast, intervertebral rotation is minimal at the curve apex, where lateral intervertebral tilting is most pronounced. The findings suggest that facet joint OA is implicated and potentially contributes to AIS progression.

Subchondral bone and cartilage are dynamic structures with complementary roles in load-bearing [16]. Unlike cartilage, which degenerates progressively, subchondral bone changes through a two-phase response, with an initial loss of bone density and reduced bone remodelling and sclerosis in the later stage [16–18]. Several mechanisms for this phenomenon have been proposed, including cartilage-bone crosstalk via subchondral pores, but this has not been explored in the context of AIS [19–21]. Degenerating cartilage releases pro-inflammatory factors that affect osteoblasts, osteoclasts, and osteocytes. The three most prominent pro-inflammatory factors in OA, IL-1, IL-6, and IL-8, can all enhance osteoclast differentiation while inhibiting osteoblasts in directly and indirectly linked pathways [22, 23]. Our previous research revealed a significant elevation of these cytokines in AIS facet joint chondrocytes [14]. The upregulation was enhanced following TLR activation [24] and supports the cartilage-bone crosstalk model. This study bypasses selecting specific factors by using unbiased deep RNA sequencing to compare chondrocyte gene expression between age-matched AIS patients with facet joint OA and non-scoliotic individuals without OA. The strategy aims to uncover key regulatory pathways in cartilage-bone crosstalk and confirm a role through functional testing. Understanding these mechanisms could provide information guiding the development of new therapies to prevent AIS progression.

Materials and methods

Collection of clinical specimens

Facet joints were collected from 35 consenting AIS patients undergoing spinal fusion surgery at the Shriner's Hospital for Children and facet joints from 16 non-scoliotic individuals (NSC) were retrieved through the Transplant Quebec Organ Donation Program. The average age was 27.6 ± 7.4 for the non-scoliotic individuals and 16.2 ± 2.6 for the AIS patients. Demographics including, age, sex, Cobb angle, and Lenke classification, along with detailed information on the experiments conducted with the specific facet joint samples can be found in Table 1. AIS facet joints resected from AIS patients depend on curve type and surgical need and include both lumbar and thoracic levels. Facet joints from organ donors were also from both thoracic and lumbar levels to ensure a similar distribution and prevent variability due to the spinal level. AIS is more frequent in females and 78% of the patients included in this study were female (Table 1). The study was approved by the McGill University institutional review board in Montreal, Canada (IRB # Tissue Biobank 2019–4896 and A03-M10-23A). Written informed consent was received before participation in the study.

Chondrocyte isolation and culture

Facet joint chondrocytes were isolated as described by Bisson et al. 2020 [24]. Briefly, facet joint cartilage was dissected from the subchondral bone, cut into small pieces and digested with Collagenase Type II (Thermo Gibco™ 17101015) for 16 h to release the chondrocytes. For RNA sequencing and baseline gene expression

Table 1 Patient Information and Applications. This table summarizes the key details of the AIS patients and NSC organ donors. The table lists each sample applied in specific experiments, as indicated with a checkmark (✓)

Sample ID	Sex	Age	COD	Apex of Curve	Lenke Type	Primary cobb angle	RNA-seq	Baseline qPCR	Baseline ELISA	TLR activation qPCR	TLR activation ELISA	Alamarblue assay	Dye-dilution	Replating +Trap quantification	EOS+ MCSF qPCR
NSC16	M	28	TBI- Brain SDH	/	/	/		✓	✓						
NSC15	F	35	Spontaneous Cerebral Hemorrhage, Hypertension, Pulmonary Embolism	/	/	/		✓	✓						
NSC1	M	16	Overdose (cocaine)	/	/	/	✓	✓	✓						
NSC2	M	20	Motor vehicle accident	/	/	/	✓	✓							
NSC14	M	31	Myocardial infarction	/	/	/		✓	✓						
NSC3	M	19	Drug overdose (alcohol, oxycodone, mirjuana)	/	/	/	✓	✓	✓						
NSC4	M	31	Drug user (Cocaine)	/	/	/			✓						
NSC5	M	22	Suicide (repeated head-handing) (automation)	/	/	/			✓						
NSC6	M	24	Motor Vehicle Accident (MVA), polytrauma	/	/	/		✓							
NSC7	M	29	NA	/	/	/		✓							
NSC8	F	33	NA	/	/	/		✓							
NSC9	M	42	NA	/	/	/		✓							
NSC10	M	27	Suicide, hanging	/	/	/		✓	✓						
NSC11	M	15	MVA (DB pers comm), brain haemorrhage	/	/	/		✓	✓						
NSC12	M	35	Anoxia (brain),Suicide (hanging)	/	/	/		✓	✓						
NSC13	M	34	Stroke CATV	/	/	/		✓							
AIS11	F	15	/	T8	6	60		✓							
AIS12	F	16	/		1	60		✓	✓						
AIS13	F	14	/	T10	2	55		✓	✓						
AIS14	F	15		T8	2	55			✓	✓	✓(P1, P2)	✓(P1, P2)	✓(P1, P2)	✓(P1, P2)	
AIS1	F	14	/	T9	1	67	✓	✓	✓	✓	✓(P1, P2)	✓(P1, P2)	✓(P1, P2)	✓(P1, P2)	
AIS2	F	16	/	T8	1	55	✓	✓	✓		✓(P1, P2)	✓(P1, P2)	✓(P1, P2)	✓(P1, P2)	
AIS3	M	15	/	T8	1	60	✓	✓	✓		✓(P1)	✓(P1)	✓(P1)	✓(P1)	
AIS15	F	17	/	T8	1	60		✓			✓(P1)			✓(P1)	
AIS16	F	16	/	T11	2	50		✓						✓(P1)	
AIS17	M	16	/	T9-10	2	66		✓						✓(P1)	
AIS18	F	15	/	T8	1	40		✓						✓(P1)	
AIS7	F	14	/	T9	2	65		✓		✓				✓(P1)	
AIS8	F	15	/	T10	2	66		✓		✓					
AIS19	F	17	/	T8	1	60		✓							
AIS20	F	14	/	T9	1	60									
AIS9	F	16	/	T9	1	50				✓					
AIS21	F	15	/	T10	2	50			✓						
AIS10	F	15	/	T8	2	65				✓					
AIS22	F	16	/	T6	1	66									✓
AIS23	F	18	/	T9	2	52									✓
AIS24	F	15	/	T9	1	56									✓
AIS25	F	16	/	T9	1	50									✓
AIS26	F	29	/	T8	1	53									✓
AIS27	F	18	/	T9	1	50									✓
AIS28	M	14	/	T7	1	55									✓
AIS29	F	16	/	T7	1	46									✓
AIS30	F	13	/	T8	2	80									✓
AIS31	F	18	/	T8	1	50									✓
AIS32	F	15	/	T8	1	85									✓
AIS33	M	17	/	T8	1	60									✓
AIS34	F	19	/	T9	1	55									✓
AIS35	F	13	/	T8	1	60									✓
AIS36	F	18	/	T8	1	50									✓
AIS37	M	19	/	T8	1	60									✓
AIS38	F	17	/	T8	1	57									✓
AIS39	M	18	/	T8	1	50									✓
AIS40	F	16	/	T8	1	60									✓

measurements, freshly isolated chondrocytes were directly lysed in TRIzol (Thermo Invitrogen™ 15596026) (Fig. 1A). In all other experiments, chondrocytes were seeded and cultured in completed Dulbecco's DMEM (Sigma Aldrich D5648), 4.5 g/L glucose, 10% FBS, 25 µg/mL gentamycin (Thermo Gibco™ 15710064), and 2 mmol/L Glutamax (Thermo Gibco™ 35050061) until they achieved 90% confluence. The conditioned media from the expansion period (P0) was collected to determine baseline cytokine release as described below. Chondrocytes at passages 1–2 were activated by the TLR-2 agonist Pam2CSK4 (InvivoGen, tlrl-pm2s-1) and TLR-4 agonist CRX-527 (InvivoGen, tlrl-crx527) at a concentration of 100 ng/mL in DMEM medium [24]. For gene expression

analysis, RNA was extracted 6 h post-TLR activation. For protein analysis, chondrocytes were exposed to TLR agonists for two days. The agonist was removed, and the cells were washed with PBS. Fresh media was added, and conditioned media was collected after a four-day period. The collected conditioned media was stored at −80 until further analysis was performed, as described below.

Deep RNA sequencing and analysis

Total RNA was extracted and 25 million paired-end reads (PE100) per sample were collected on the NovaSeq 6000 platform (Illumina, Inc.). Raw reads were evaluated by FASTQC (Galaxy Version 0.74 + galaxy0) followed by trimming to remove adapter sequences (Trimmomatic (Galaxy Version 0.39 + galaxy0)). Cleaned reads were aligned to the reference genome using HISAT2 (Galaxy Version 2.2.1 + galaxy1) with gh38 reference genome. FeatureCounts (Galaxy Version 2.0.3 + galaxy2) quantified expression levels from aligned reads. Differential expression analysis was evaluated with the Limma package (Galaxy Version 3.50.1 + galaxy0). Sex-specific genes, 93 Y-linked and 52 X-linked genes, were omitted from the DEG. Normalized counts (CPM) was obtained and Limma DEG analysis was employed to conduct GSEA on gene sets from the HALLMARK, REACTOME, and WIKIPATHWAY databases. Functional annotation of significant DEGs was achieved through Gene Ontology (GO) analysis using the ShinyGO platform (Version 0.77). The STRING database was used to identify protein–protein interaction (PPI) networks. PPI's were visualized and analyzed in Cytoscape (3.10.1), where MCODE was used for clustering analysis and CytoHubba for topological evaluations (Fig. 1A).

RTqPCR

RNA was extracted and reverse transcription of 1 µg RNA was performed as described in [24]. Gene expression was calculated using ß-actin and RPL13A as housekeeping genes, normalizing target gene Ct values against the geometric mean of the two reference genes and presented as relative expression using the $2^{\wedge -\Delta\Delta Ct}$ method (primers Table 2).

Cartilage morphological grading and EOS 3D reconstruction

High-resolution photographs were acquired with a Canon EOS 5D Mark II camera with a Canon F2.8 100mm Macro L lens. The gross morphological appearance of the cartilage was classified according to Li et al. [25] by two independent observers. Grade 0 = normal; Grade 1 = surface fibrillation; Grade2 = fissuring; Grade 3 = erosion of 30% or less of the articular surface; Grade 4 = erosion of more than 30% of the articular surface. For the same patients, three-dimensional (3D) spine reconstructions were generated from bi-planar radiographs acquired 2–6 weeks before surgery as described by Bisson et al. [15]. Briefly, pre-operative biplanar low-dose radiographs of the spines were analyzed in 3D using the EOS software. First, the pelvic parameters were identified, the software then simulated the thoracic and lumbar vertebrae, and the examiner aligned, positioned, and adjusted each vertebra to match the biplanar radiographs as closely as possible. Two independent evaluators reconstructed the spines at three different times. The scores from 6 reconstructions were averaged for the final analysis. To evaluate the similarity of reconstructions between the two evaluators, all 3D parameters were plotted and evaluated with the Bland–Altman analysis. The scatter plot and histogram showed a strong correlation and a high degree of overlap. (Supplementary Fig. 5).

Multiplex ELISA

Mobile factors were determined in conditioned media from p0 and p1-2 chondrocytes with and without TLR activation. A customized multiplex ELISA was used to quantify IL-1a, IL-6, IL-8, IL-17a, CXCL-1, CXCL-10, M-CSF, GM-CSF, RANKL, TNF-alpha, OPG, and IFN-gamma (kit number: PPX-16-MXYMKA3). The analysis was conducted according to the manufacturer's instructions.

(See figure on next page.)

Fig. 1 Expression profiling of facet joint chondrocytes identified AIS-associated gene and regulatory networks. **A** Schematic representation of the RNA sequencing workflow, from sample processing to bioinformatic analysis (NSC *n*=3; age=18.3±1.7 AIS *n*=3; age=15±1). **B** The Volcano plot illustrates genes with $P < 0.05$ and |Log FC| > 1 in red, comparing AIS chondrocytes to NSC.**C** Venn diagram numerically illustrates DEGs in AIS compared to NSC: upregulated (red), downregulated (blue), and unchanged genes (overlap). **D** The heatmap shows a clear separation of significant DEGs, between AIS and NSC chondrocytes: red for higher and blue for lower expression levels. **E**, **F** The lollipop plot represented GO pathway enrichment and biological processes for upregulated DEGs. Each sphere size reflects the count of involved genes, while the red-to-cyan gradient represents *p*-value ranges. The x-axis shows the fold enrichment for each term. **G** The multi-GSEA plot illustrates enriched pathways from HALLMARK, REACTOME, and Wiki_Pathway databases, identifying significant biological processes impacted in AIS. **H** The PPI network, constructed using Cytoscape, reveals significant modules within cluster-1. The top 20 genes by Maximum Neighborhood Component (MNC) are colour-coded from red to orange, with blue dots representing their first connected genes. Figure layout designed using the BioRender.com platform

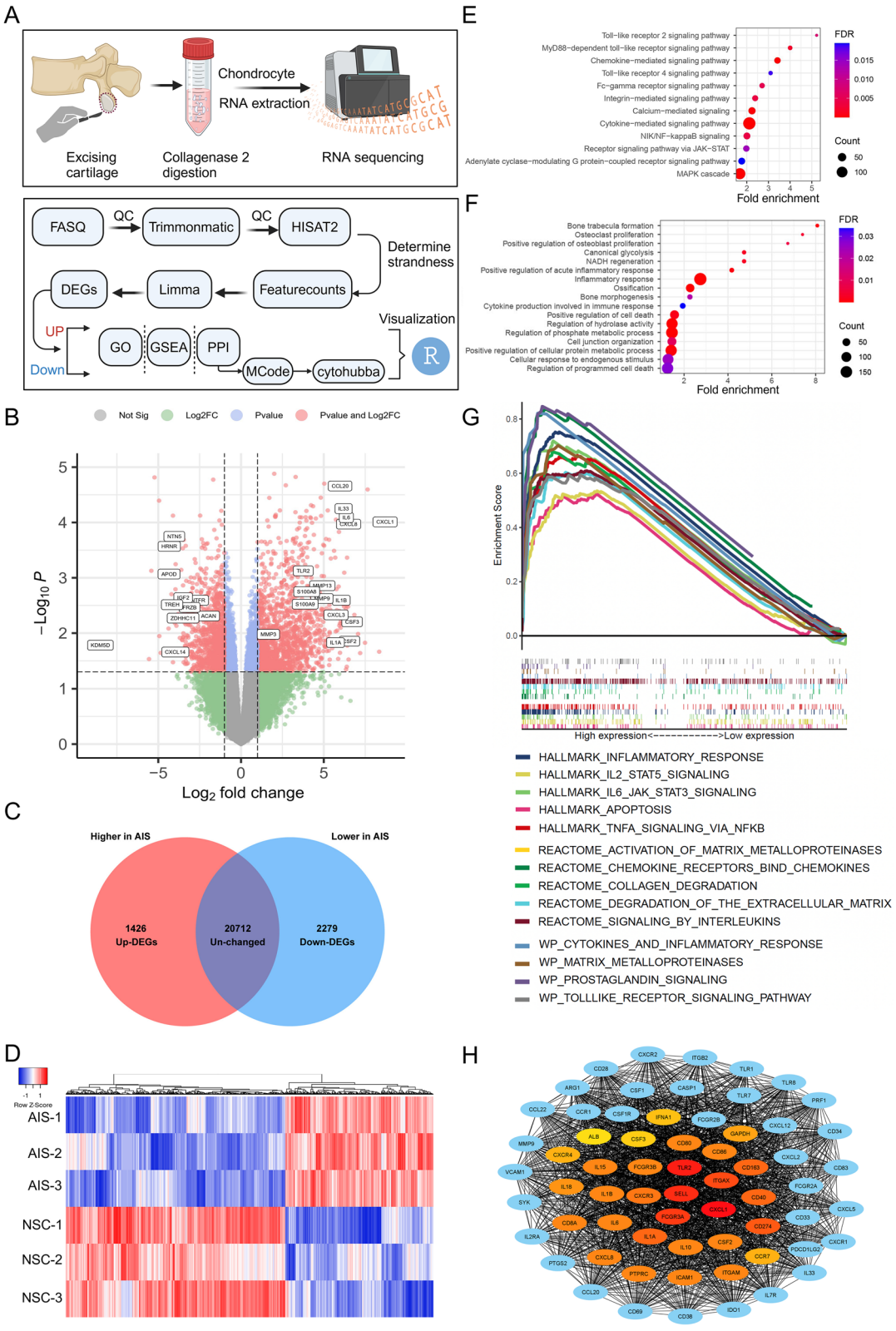

Fig. 1 (See legend on previous page.)

Table 2 List of Primer Sequences Used in This Study. This table provides the 5′—3′sequences of all primers utilized in the experiments described in this paper

Gene	Forward Primer (Sequence (5' -> 3'))	Reverse Primer Sequence (3' -> 5')
TLR1	CAG TGT CTG GTA CAC GCA TGG T	TTT CAA AAA CCG TGT CTG TTA AGA GA
TLR2	ATCCTCCAATCAGGCTTCTCT	GGACAGGTCAAGGCTTTTTACA
TLR4	CAG AGT TTC CTG CAA TGG ATC A	GCT TAT CTG AAG GTG TTG CAC AT
TLR6	GAA GAA GAA CAA CCC TTT AGG ATA GC	AGG CAA ACA AAA TGG AAG CTT
RANKL	CAA CAT ATC GTT GGA TCA CAG CA	GAC AGA CTC ACT TTA TGG GAA CC
GM-CSF	TCCTGAACCTGAGTAGAGACAC	TGCTGCTTGTAGTGGCTGG
M-CSF	TGGCGAGCAGGAGTATCAC	AGGTCTCCATCTGACTGTCAAT
OPG	GCGCTCGTGTTTCTGGACA	AGTATAGACACTCGTCACTGGTG
CXCL-1	GCCCAAACCGAAGTCATAGCC	ATCCGCCAGCCTCTATCACA
CXCL10	GTGGCATTCAAGGAGTACCTC	TGATGGCCTTCGATTCTGGATT
IFN-Y	AAC-TAC-TGA-TTT-CAA-CTT-CT	ATT-ACT-GGG-ATG-CTC-TTC
TNF-A	ATGTTGTAGCAAACCCTCAAGC	TCTCTCAGCTCCACGCCATT
CXCL-5	AGCTGCGTTGCGTTTGTTTAC	TGGCGAACACTTGCAGATTAC
CXCL-12	ATTCTCAACACTCCAAACTGTGC	ACTTTAGCTTCGGGTCAATGC
CXCL-2	CTGCTCCTGCTCCTGGTG	AGGGTCTGCAAGCACTGG
CCL-2	GCATGAAAGTCTCTGCCG	GAGTGTTCAAGTCTTCGGA
CCL-3	AGTTCTCTGCATCACTTGCTG	CGGCTTCGCTTGGTTAGGAA
CCL-5	GAAGGTCTCCGCGGCAGCC	CTGGGCCCTTCAAGGAGCGG
CCL-7	CACTTCTGTGTCTGCTGCTCAC	GTTTTCTTGTCCAGGTGCTTCATA
CCL-8	GCCTGCTGCTCATGGCAGCC	GCACAGACCTCCTTGCCCCG
CCL-4	CTGTGCTGATCCCAGTGAATC	TCAGTTCAGTTCCAGGTCATACA
CCL-11	CCCCTTCAGCGACTAGAGAG	TCTTGGGGTCGGCACAGAT
CCL-20	TGCTGTACCAAGAGTTTGCTC	CGCACACAGACAACTTTTTCTTT
IL-1A	AGATGCCTGAGATACCCAAAACC	CCAAGCACACCCAGTAGTCT
IL1B	ATGATGGCTTATTACAGTGGCAA	GTCGGAGATTCGTAGCTGGA
IL-6	TGA ACC TTC CAA AGA TGG CTG	CAA ACT CCA AAA GAC CAG TGA TG
IL-7	AGATTACTACAACCGATCCACCT	GGGGACAGAGTTCATGTGGTA
IL-11	CGAGCGGACCTACTGTCCTA	GCCCAGTCAAGTGTCAGGTG
IL-15	TTTCAGTGCAGGGCTTCCTAA	GGGTGAACATCACTTTCCGTAT
IL-8 (CXCL-8)	TCC TGA TTT CTG CAG CTC TG	GTC TTT ATG CAC TGA CAT CTA AGT TC
IL-17	AGATTACTACAACCGATCCACCT	GGGGACAGAGTTCATGTGGTA
IL-23	CTCAGGGACAACAGTCAGTTC	ACAGGGCTATCAGGGAGCA
IL-3	CAGACAACGCCCTTGAAGACA	GCCCTGTTGAATGCCTCCA
IL-4	CCAACTGCTTCCCCCTCTG	TCTGTTACGGTCAACTCGGTG
IL-10	GACTTTAAGGGTTACCTGGGTTG	TCACATGCGCCTTGATGTCTG
IL-27	ACCGCTTTGCGGAATCTCA	AGGTCAGGGAAACATCAGGGA
IL-33	GTGACGGTGTTGATGGTAAGAT	AGCTCCACAGAGTGTTCCTTG
TGF-B1	TCCTGGCGATACCTCAGCAA	CTCAATTTCCCCTCCACGGC
ACTB	GTC TTC CCC TCC ATC GTG G	AAT CCT TCT GAC CCA TGC C
RPL13	AAAAAGCGGATGGTGGTTC	CTTCCGGTAGTGGATCTTGG

Osteoclast formation assays

Bone marrow cells were isolated from long bones of 4-month-old C57BL/6J mice. All procedures were approved by the McGill University Animal Care Committee (protocol #7127) and were conducted in compliance with the ethical guidelines of the Canadian Council on Animal Care [26]. Red blood cells were removed with RBC lysis buffer (Thermo AAJ62990AK), and bone marrow cells were cultured in MEM α (Thermo Gibco™ 41061029) media with 1% sodium pyruvate (Thermo Gibco™ 11360070), 10% fetal bovine serum 10,000 IU penicillin and 10,000 µg/ml streptomycin (Thermo Gibco™ 15140122). Isolated cells were plated and primed with MCSF (50 ng/ml) (PeproTech, 300–25-250UG) for 24 h. Primed cells were then seeded at a density of 5×10^3 cells/cm^2. The cells were cultured in Osteoclastogenic media composed of α MEM supplemented with MCSF (30ng/ml) and RANKL (80 ng/ml) (PeproTech, 310–01-250UG) for 4–7 days, replacing the media every two days. Following the culture period, samples were fixed using 4% methanol-free paraformaldehyde (Thermo 043368.9M). TRAP staining was performed according to the manufacturer's instructions (Sigma 387A-1KT). Osteoclast differentiation was quantified by counting TRAP-positive cells containing more than three nuclei.

Metabolic activity assay and dye dilution assay

Osteoclast precursors were exposed to chondrocyte-CM (CCM) or unconditioned chondrocyte media (UCM) in osteoclastogenic media, at a ratio of 1:4 (Supplementary Fig. 3). Metabolic activity was determined post-treatment using the alamarBlue™ Cell Viability Reagent (Thermo DAL1025) according to the manufacturer's instructions. The proliferation rate was measured using the CellTrace™ Violet Cell Proliferation Kit (C34571), according to the manufacturer's protocol. Briefly, dyed cells were seeded at a density of 5×10^3 cells/cm^2 and cultured for 4 days in the presence of CCM, without TLR pre-activation. Data on fluorescent intensity was acquired through flow cytometry and analyzed in FlowJo (version 10.8.1).

Statistical analysis

There are no prior studies investigating the expression of bone remodelling genes in facet joint chondrocytes that could be used for power analysis. We therefore analyzed eight genes of interest from the current deep RNA sequencing that met the criteria for both *p*-value and log fold change (LogFC), including M-CSF, GM-CSF, IL1a, IL1b, IL-6, IL-8, CXCL-1, CXCL-10. The estimated effect size, expressed as Cohen's d, was calculated using the formula: $d \approx \frac{2\sqrt{-\ln(p)}}{\sqrt{n}}$ (p represents the *p*-value, and n is the total sample size). The range of estimated Cohen's d for the analyzed genes was between 1.23 and 2.50, indicating a large effect size across all comparisons. For a desired statistical power level of 80% and a significance level (alpha) of 0.05, the estimated minimum sample size per group (for a two-tailed hypothesis test) ranged from 4 to 12, depending on the specific effect size observed for each gene (a-priori sample size calculator for student t-Tests from Free Statistics Calculators version 4.0). For the correlation of 3D parameters, our previous study determined that a minimum of 16 facet joint pairs needed to be analyzed for each parameter to observe the desired effect [15].

The Shapiro–Wilk test was performed to assess the normality of all datasets. When comparing two groups, parametric data were analyzed using a two-tailed unpaired t-test, while nonparametric data were analyzed using a two-tailed unpaired Mann–Whitney test. For multiple comparisons involving more than two groups, one-way ANOVA with Dunnett's T3 multiple comparisons test was used for parametric data, and the Kruskal–Wallis test was applied for nonparametric data. Spearman correlation analysis was applied to determine the relationship between MCSF gene expression, cartilage morphological grading, and intervertebral angles across all selected spinal levels. All statistical analyses were calculated using GraphPad Prism 10. Significance defined by $^{*}P<0.05$, $^{**}P<0.01$, $^{***}P<0.001$, $^{****}P<0.0001$.

Results

Gene expression profiling identified AIS-associated regulatory gene networks

Deep RNA-seq was used to find differentially expressed genes (DEGs) in facet joint chondrocytes from a limited number of AIS and age-matched non-scoliotic individuals, as schematically depicted in (Fig. 1A). A volcano plot of the complete set of 24,417 genes was generated based on *P* value < 0.05 and |Log2FC| > 1 (Fig. 1B). 1426 genes were significantly Up-DEGs, in AIS chondrocytes, whereas 2279 genes were significantly Down-DEGs (Fig. 1C). The heatmap and principal component analysis (PCA) visually present the expression pattern with a distinct separation between AIS and non-scoliotic control samples (Fig. 1D, Supplementary Fig. 1B).

GO functional enrichment analysis determined pathways and biological processes implicated by the Up-DEGs and Down-DEGs. Up-DEGs were enriched in signalling pathways, with a particular emphasis on the Toll-Like Receptor 2 (TLR2) (FDR = 7.76E-03) and Toll-Like Receptor 4 (TLR4) signalling pathways (FDR = 1.88E-02). Several interconnected pathways were present, including the MAPK cascade (FDR = 3.07E-06), NIK/NF-kappaB signalling pathway (FDR = 4.027E-03), cytokine-mediated signalling pathway (FDR = 3.51E-15), Chemokine-mediated signalling pathway (FDR = 3.06E-06) and MyD88-dependent TLR signalling pathway (FDR = 2.08E-03). In concordance with the enriched pathways, a pronounced enrichment of biological processes associated with inflammation and cytokine production was evident (Fig. 1E). Furthermore, GO terms linked to bone remodelling were enriched and exhibited remarkably high FDR-adjusted *p*-value, including bone morphogenesis (FDR = 3.41E-06), ossification (FDR = 8.62E-07), positive regulation of osteoblast proliferation (FDR = 1.06E-07), osteoclast proliferation (FDR 1.01E-08), and bone trabecula formation (FDR = 4.92E-10) (Fig. 1F). GSEA analysis of the HALLMARK gene sets indicated that the most prominent pathway was in inflammatory response, with an enrichment score (ES) of 0.75. We also observed a significant enrichment in pathways including IL-2/STAT5 signalling (ES = 0.66), IL-6 JAK/STAT3 signalling (ES = 0.76), apoptosis (ES = 0.56), and TNF-alpha signalling (ES = 0.61). The REACTOME gene set identified pathways associated with matrix degradation, including activation of matrix metalloproteinases (MMPs) (ES = 0.66), collagen degradation (ES = 0.66), degradation of ECM (ES = 0.66), in addition to interleukin signalling (ES = 0.74), and chemokine receptor binding chemokines (ES = 0.74). Lastly, within the WIKIPATHWAY gene set, we identified similar pathways linked to inflammation, such as cytokines and inflammatory response (ES = 0.74), matrix metalloproteinases (ES = 0.74), prostaglandin

signalling (ES = 0.74), and TLR signalling pathway (ES = 0.74) (Fig. 1G).

The PPI networks of the up-DEG network comprise 1146 nodes and 27,666 edges. Densely connected gene clusters within the network were visualized using MCODE v1.32 (Supplementary Fig. 1 A). The top three clusters share KEGG pathways related to cytokines, chemokines, and the TLR and NFκB pathways (Supplementary Fig. 1C). Cluster 1 had the strongest FDR and greatest number of enriched proteins, underscoring its key role in the suggested pathways. To further explore hub genes within Cluster 1, we utilized the CytoHubba plugin for a detailed topological analysis, ranking genes using scores such as Maximum Neighborhood Component (MNC), Density of Maximum Neighborhood Component (DMNC), and Maximal Clique Centrality (MCC). As shown in Fig. 1H proteins are displayed in a gradient from red to yellow. The top ten, ranked by MNC from highest to lowest, are CXCL-1, TLR2, SELL, FCGR3, AITGAX, CD274, CD163, IL-1A, CD40, CXCR3. Notably, TLR2 consistently ranked as a top hub gene across multiple topological analyses.

Our in-depth transcriptomic analysis suggests the involvement of TLR-related pathways in facet joint osteoarthritis (OA) and TLR-related genes with regulatory roles in bone remodelling.

Validation of genes with function in bone turnover

We performed qPCR in a larger cohort of AIS and non-scoliotic control chondrocytes to validate the suggested association with the TLR pathway. In line with our previous publication, AIS chondrocytes had a significantly higher baseline gene expression of TLR2 (FC = 15.7, $p < 0.0001$), with no significant difference in TLR1, 4 and 6 expression in comparison to non-scoliotic chondrocytes (Supplementary Fig. 2).

The gene expression level of various downstream cytokines and chemokines implicated in bone remodelling were significantly higher in AIS chondrocytes at baseline, including the pro-osteoclastogenic factors, RANKL (FC = 18.4, $p = 0.0006$), M-CSF (FC = 5.0, $p = 0.0004$), GM-CSF (FC = 4.2, $p = 0.0007$), IL-1α (FC = 25.5, $p < 0.0001$), IL-8 (FC = 5.1, $p = 0.0010$), IL-6 (FC = 12.1, $p = 0.0257$), CXCL-1 (FC = 12.1, $p = 0.0198$), CXCL-10 (FC = 8.5, $p = 0.0233$), TNF-α (FC = 4.0, $p = 0.0008$). Among the assessed genes, IL-17 and INF-γ showed no differences between the two groups. Unexpectedly, the anti-osteoclastogenic factor OPG exhibited a 5.9-fold higher expression, $p = 0.0029$, in AIS chondrocytes (Fig. 2A).

The level of cytokines and chemokines in chondrocyte-conditioned culture media were measured using multiplex ELISA, to determine if protein concentration correspond with gene expression. (Fig. 2B) Consistent with the RNAseq and qPCR data, a significant elevation of RANKL (FC = 1.5, $p = 0.01$), M-CSF (FC = 2.2, $p = 0.0158$), GM-CSF (FC = 1.3, $p = 0.0498$), IL-1α (FC = 3.1, $p = 0.0185$), IL-8 (FC = 6.3, $p = 0.0285$), CXCL-1 (FC = 10.9, $p = 0.0347$), IFN-γ (FC = 1.6, $p = 0.0182$), and TNF-α (FC = 2.0, $p = 0.0262$) were detected in CM from AIS chondrocytes. IL-6 (FC = 12.1, $p = 0.0536$) showed a trend of higher protein concentration in AIS chondrocytes but did not reach statistical significance. OPG, CXCL-10 and IL-17 did not show a difference between the two groups.

TLR activation-induced production of pro-osteoclastogenic factors

Based on the GO analysis suggesting an involvement of TLR-related pathways and pathways with regulatory roles in bone remodelling, synthetic agonists for TLR 2 and 4 were applied to determine a potential link between TLR activation and bone remodelling. TLR genes and a panel of 40 cytokines and chemokines with a role in bone remodelling were selected (Fig. 3A). Among these genes, 30 are pro-osteoclastogenic (pro-OC), while 10 are anti-osteoclastogenic (anti-OC). Most pro-OC genes exhibited a strong induction upon both TLR2 and TLR4 activation, with the overall fold induction being, on average, higher compared to anti-OC genes. This pattern suggests a shift in the secretory profile that may favor osteoclastogenesis upon TLR activation. Specifically, MCSF, GMCSF, CXCL-5, CXCL-8, CXCL-10, CXCL-12, CX3CL-1, CCL-2, CCL-3, CCL-4, CCL-7,CCL-8,CCL-20, IL-1β, IL-8, IL-6, and IL-15 showed a statistically significant induction in response to both agonists. Other pro-OC genes, while trending upwards, did not reach statistical significance potentially due to a high baseline expression in some patients. In contrast, no anti-OC genes showed statistically significant induction

(See figure on next page.)

Fig. 2 Validation of TLRs and inflammatory factors with known function in regulating bone turnover. **A** Baseline gene expression of bone regulatory cytokines in AIS (n = 10–11 age=15.4 ±0.9) and NSC (n = 12 age=27.7±7.7) facet joint chondrocytes. Data was analyzed using a two-tailed Mann–Whitney U test. **B** Bone regulatory cytokines secretion in conditioned culture media from primary AIS (n = 7 age=15.1±0.8) and NSC chondrocytes (n = 7 age=27.6±6.7). Data was analyzed using a two-tailed t-test. Significance defined by *P< .05, **P< .01, ***P< .001,****P<0.0001. Figure layout designed using the BioRender.com platform

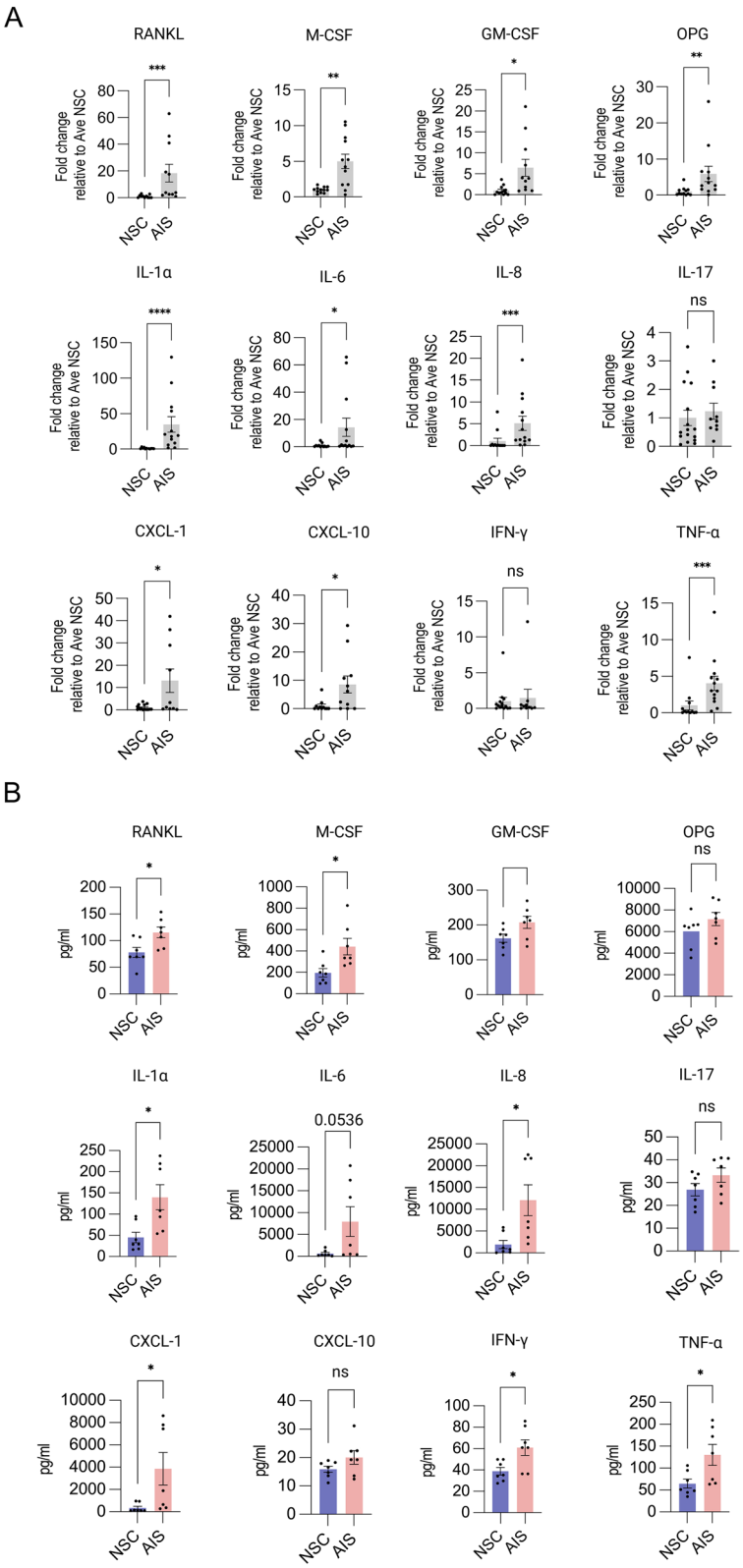

Fig. 2 (See legend on previous page.)

upon TLR activation. We also observed a statistically significant induction in TLR2 gene expression in response to TLR2 and TLR4 agonists.

A multiplex ELISA assay was conducted to capture cumulative protein secretion. Protein secretion followed gene expression with significantly higher cytokine concentration in conditioned media following TLR2 and TLR4 activation (Fig. 3B). The TLR2-activated group displayed a wider range of values that frequently peaked at higher levels than the TLR4-activated group. The factors IL-1α, IL-6, IL-8 and OPG showed significantly higher concentrations when comparing TL2 to TLR4-activation.

TLR-activated chondrocyte-conditioned media enhanced osteoclast precursor proliferation

M-CSF and GM-CSF are pivotal regulators of osteoclast precursor proliferation. Both were strongly implicated in the GO analysis and in the subsequent gene and protein expression validated their expression. We therefore assessed the effect of chondrocyte-CM (CCM) on osteoclast precursor proliferation. Metabolic activity of osteoclast precursor cells was measured after 48, 72 and 96 h of exposure to CCM or unconditioned culture media (UCM) (Fig. 4A). We observed a 39% increase in metabolic activity ($p=0.002$) in osteoclast precursors when exposed to CM as early as 48 h. This trend was continuously enhanced at the 72-h (63% increase, $p=0.004$) and 96-h time points (73% increase, $p=0.003$). The effect was further enhanced when osteoclast precursor cells were exposed to CM from AIS chondrocytes pre-activated with TLR2 or 4 agonists (TLR2A-CCM, TLR4A-CCM). Osteoclast precursor cells exposed to TLR2A-CCM resulted in a 55% increase ($p<0.001$) and TLR4A-CCM a 67% increase ($p=0.004$) after 48 h. The increase was a 208%, in the TLR2-CCM group($p<0.001$) and 200% increase ($p<0.001$) TLR4A-CCM group at 72 h. By 96 h, the increase was 204% ($p=0.002$) in the TLR2A-CCM group and 224% ($p<0.001$) in the TLR4-CCM group (Fig. 4B, C, D). We then used a dye dilution assay to validate that the increase in metabolic evaluation was due to proliferation. A pronounced drop in dye intensity was observed when osteoclast precursors were exposed to CCM (40% decrease, $p=0.0031$). The reduction was stronger and more significant when the osteoclast precursors were exposed to TLR2A- or TLR4A-CCM. Specifically, TLR2A-CCM resulted in a 53% decrease ($p<0.0001$), and TLR4A-CCM resulted in a 59% decrease in fluorescence ($p<0.0001$). This decrease implies an increased proliferation rate as the dye diminishes with cell division (Fig. 4E, F). Collectively, the data revealed that osteoclast precursors have an accelerated proliferation rate when exposed to CCM from AIS chondrocytes, which was more robust and significant when the AIS chondrocytes were pre-activated with TLR agonists.

TLR-activated chondrocyte-conditioned media enhanced mature osteoclast formation

We then determined if the observed increased osteoclast precursor cell proliferation translated to an enhanced formation of multinucleated mature osteoclasts. In vitro osteoclastogenesis is profoundly influenced by cell density. In pilot experiments, exposure to CCM from AIS chondrocytes led to an increased number of $TRAP^+$ mononuclear osteoclast precursors. However, the over-confluency prevented multinucleation. (Supplementary Fig. 4). We modified the approach to exclude the potential artificial inhibitory effect potentially arising from high confluency. Osteoclast precursor cells were exposed to CCM for 4 days; they were then replated at a cell density optimal for fusion (Fig. 5A). Within 1–3 days, multinucleation was evident in all groups. We observed a slightly higher density of multinucleated $TRAP^+$ osteoclasts in CCM-treated wells, but the multinucleated $TRAP^+$ osteoclast size remained smaller (Fig. 5B). Quantification of multinucleated $TRAP^+$ cells showed that exposure to CCM resulted in a 2.2-fold increase in the total number of multinucleated osteoclasts ($p=0.0076$) compared to UCM. Exposure to TLR-CCM resulted in an even higher increase: 3.0-fold for TRL2A-CCM ($p<0.0001$) and 3.1-fold for TLR4A-CCM ($p=0.0002$). The number of multinucleated osteoclasts in the TLR2A-CCM and TLR4A-CCM groups were higher than the CCM group but did not reach statistical significance. (Fig. 5C). Our results suggest that TLR activation of AIS-chondrocytes affects bone homeostasis by promoting osteoclastogenesis.

(See figure on next page.)

Fig. 3 TLR activation-induced production of pro-osteoclastogenic factors. **A** The heatmap displays the fold induction for a gene panel of 40 bone regulatory cytokines and TLR 1,2,4, 6 following pre-treatment with TLR2 agonist (TLR2-A) and TLR4 agonist (TLR4-A) in primary chondrocytes ($n = 6$). Red colour indicates an upregulation, while blue represents a suppression of the gene expression. "X" means the gene expression was not detected. Data was analyzed using a two-tailed Mann–Whitney U test. **B** Bone regulatory cytokine secretion analysis of chondrocyte conditioned media collected 4 days after TLR2 or 4 activation (n=8). Data was analyzed using Kruskal-Wallis test. Significance defined by *P< .05, **P< .01, ***P< .001, ****P<0.0001. Figure layout designed using the BioRender.com platform

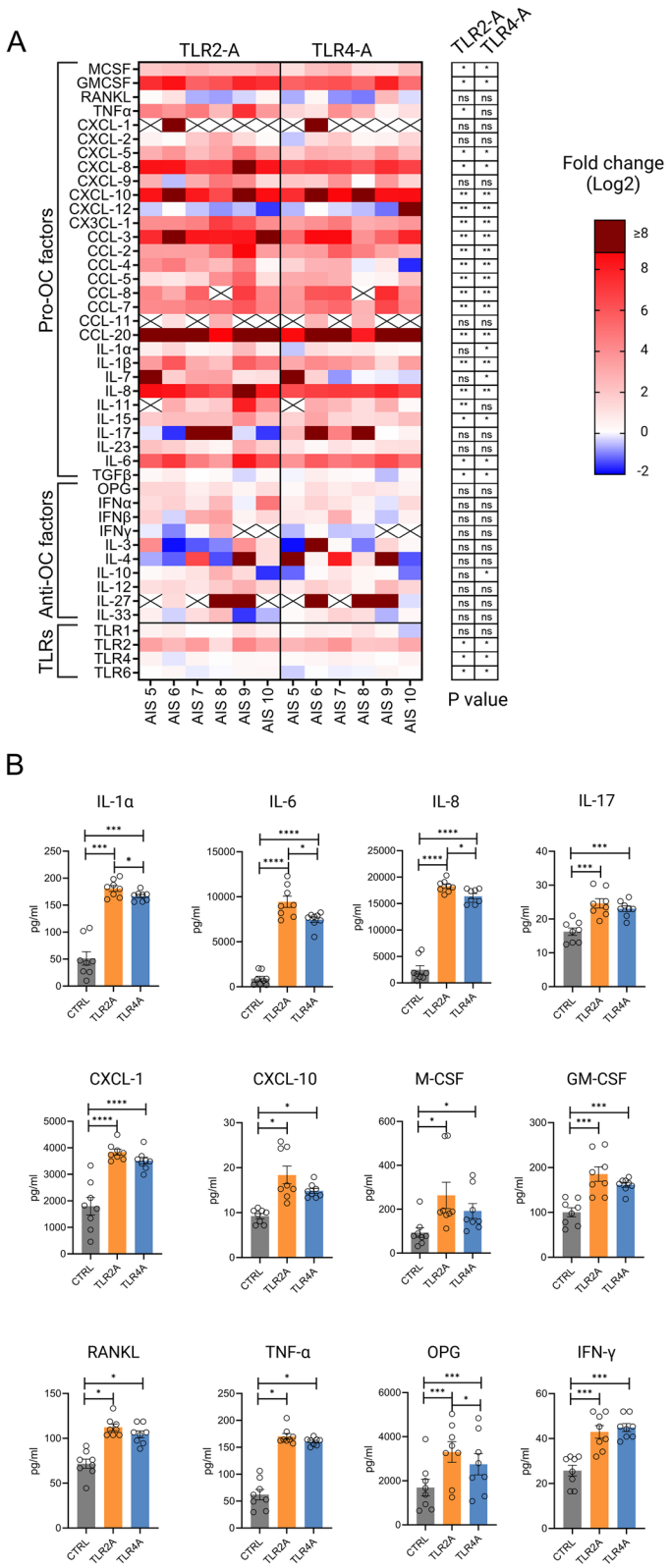

Fig. 3 (See legend on previous page.)

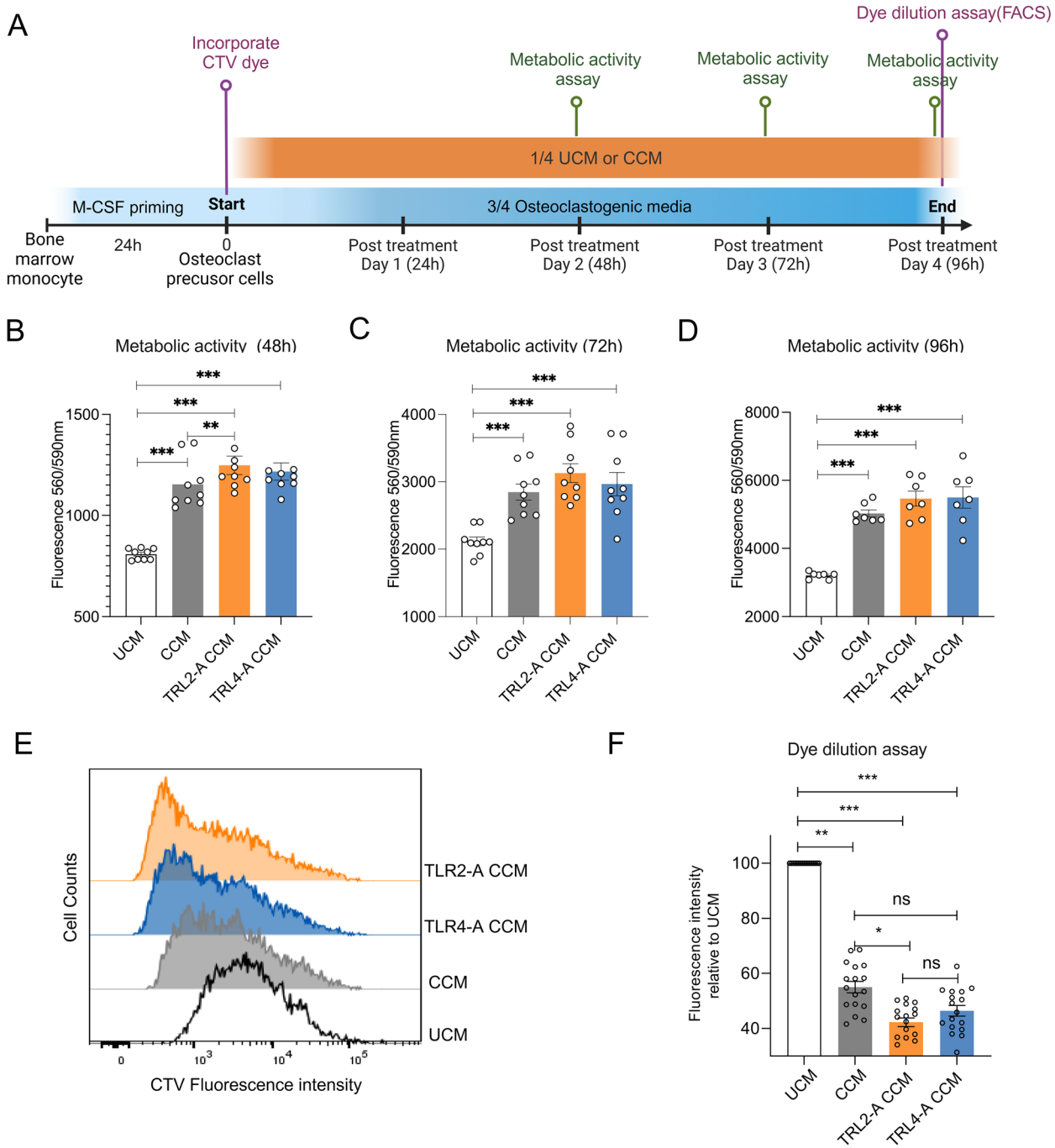

Fig. 4 TLR-activated chondrocyte-conditioned media enhanced osteoclast precursor proliferation. **A** Schematic overview of the experimental setup for monitoring proliferation during osteoclastogenesis. **B-D** Metabolic activity of osteoclast precursor cells 24–96 hours after exposure to CCM, with or without pre-activation by TLR2 or TLR4 agonists. Data was analyzed using ANOVA with Dunnett's T3 multiple comparisons test **E**. Representative histogram of CellTrace Violet dye-labelled osteoclast precursors cultured for 4 days with or without exposure to CCM, TLR2-CCM, or TLR4-CCM. **F** Quantification of the geometric mean of CellTrace Violet dye fluorescent intensity. (Patients CM n=7, Mice batch$n$=2). Data was analyzed using Kruskal-Wallis test. Significance defined by *$P < .05$, **$P < .01$, ***$P < .001$, ****P<0.0001. Figure layout designed using the BioRender.com platform

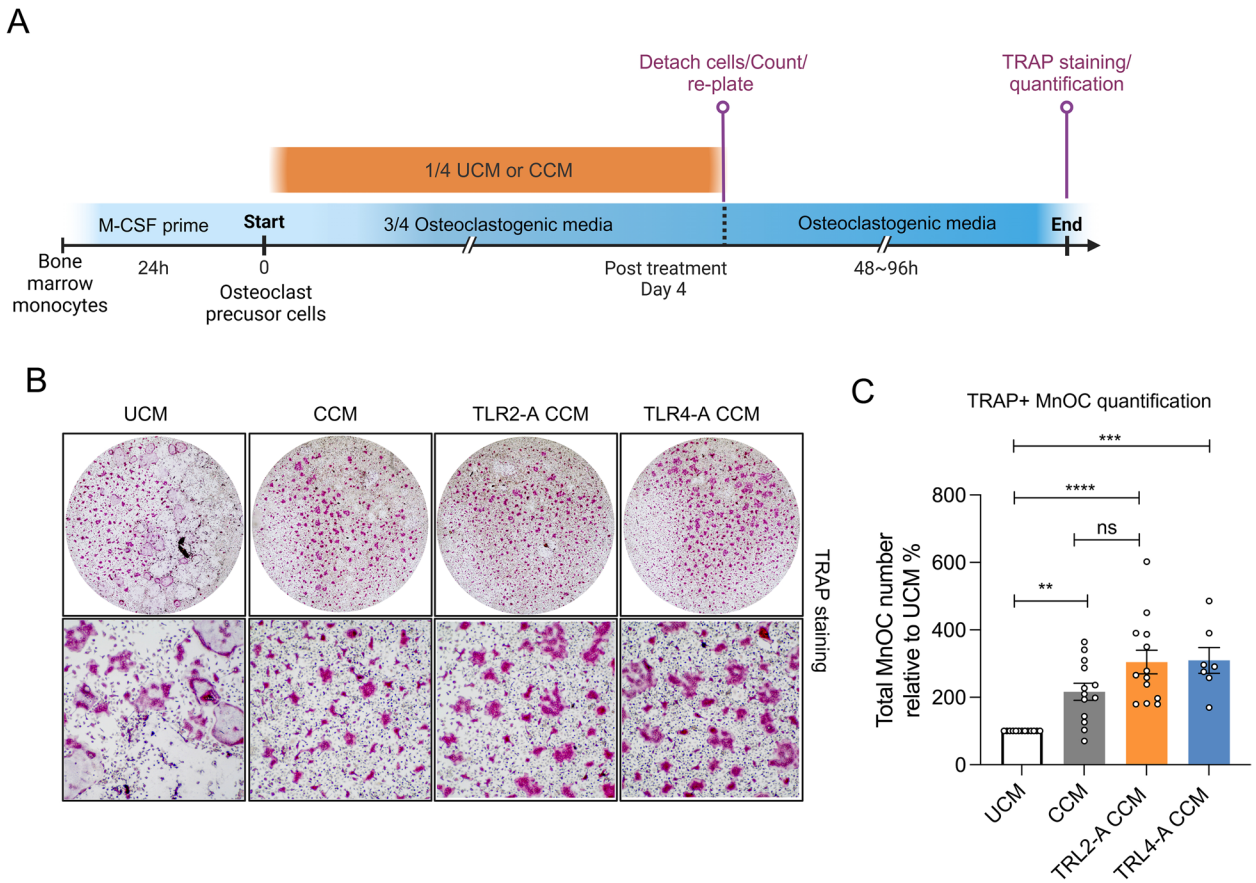

Fig. 5 TLR-activated chondrocyte-conditioned media enhanced osteoclast formation and maturation. **A** Schematic overview of the modified osteoclastogenesis procedure. osteoclast precursor cells were replated 4 days after exposure to CCM.) **B** Representative image of TRAP staining of replated osteoclasts. **C** Quantification of the total number of multi-nuclear osteoclasts (MnOC) (nuclei number >=3) for each condition. (Patients CM *n*=7–12). Data was analyzed using Kruskal-Wallis test. Significance defined by **P* <.05, ***P* < .01, ****P* < .001, *****P*<0.0001. Figure layout designed using the BioRender.com platform

Increased M-CSF gene expression correlated with more severe OA and greater intervertebral rotation

As M-CSF was expressed at a significantly higher level in AIS chondrocytes compared to non-scoliotic control cells and based on our previous finding of more severe OA appearing above and below the apex, we set out to analyze if the elevated M-CFS expression correlated with OA severity and intervertebral rotation at these specific locations [14, 15]. Facet joint chondrocytes were isolated from the levels as indicated in Fig. 6A. M-CSF gene expression was higher above and below the apex, 3.2-times ($p<0.0001$) higher above and 1.8-times higher ($p=0.0192$) below the apex(Fig. 6B). A higher M-CSF expression coincided with a significantly higher degeneration grade, 1.2 grade higher at above ($p<0.0001$) and 1.1 grade higher at below ($p<0.0001$) (Fig. 6C). In line with our previous study, axial intervertebral rotation was higher above and below the apex, 5.9 degrees ($p<0.0001$) above and −4.2 degrees ($p<0.0001$) below the apex (Fig. 6D). Further, the Spearman correlation revealed that the M-CSF expression correlates with morphological grade and axial intervertebral rotation but not with sagittal and coronal intervertebral angle (Fig. 6E, F).

Discussion

Subchondral bone deterioration is a hallmark of OA and manifests with a loss of underlying bone in the early stage, and sclerosis in the later stages. Our prior study showed a significant correlation between the severity of cartilage degeneration and the reduction of subchondral bone quality in facet joints of AIS patients like that found in early OA of adult patients [15, 27]. A similar association was found in the lumbar facet joints in a mouse model of facet joint OA [28]. Collectively, the pathological alterations in cartilage and bone may negatively impact the growth modulation of the facet joints, resulting in reduced rotational stability of the spine and possibly contributing to the progression of scoliosis [15].

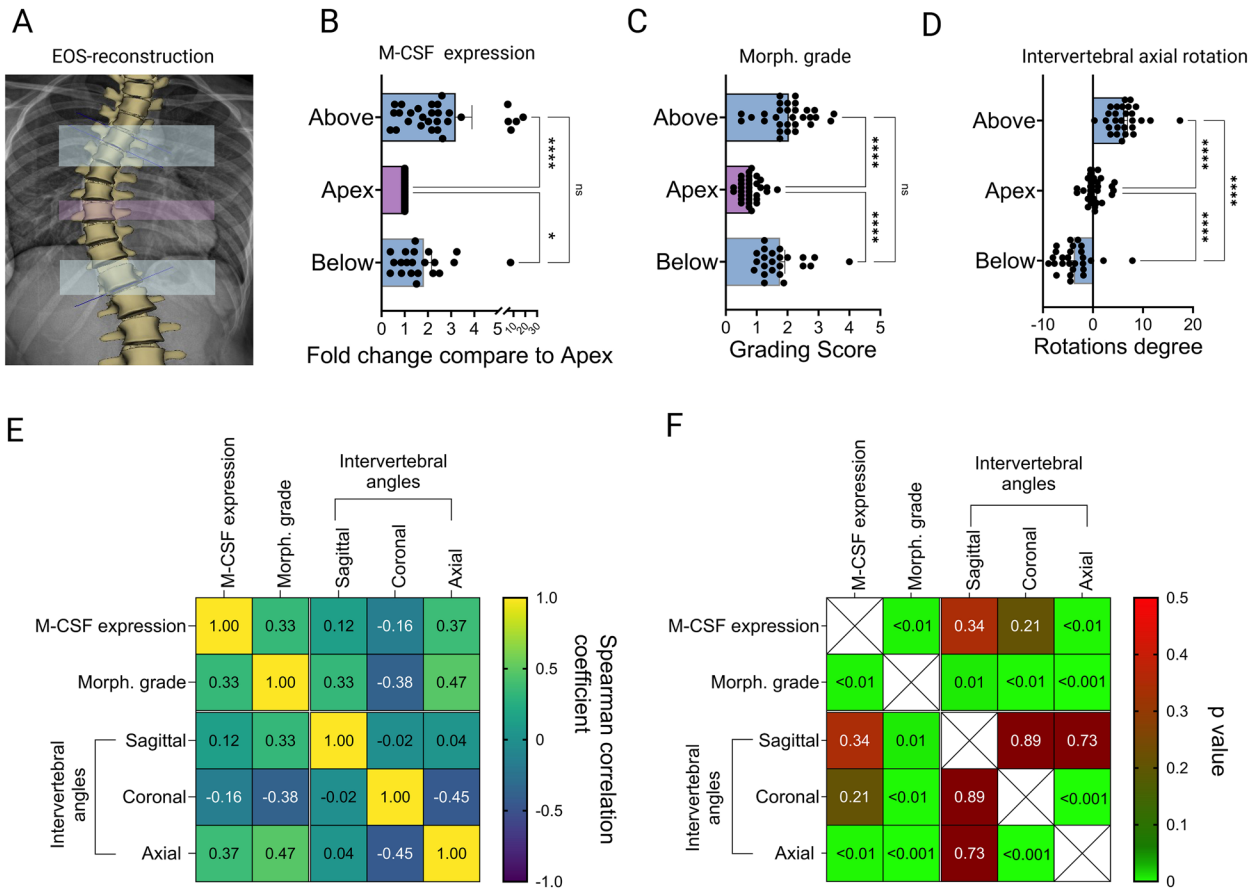

Fig. 6 Increased M-CSF gene expression in facet joints with more severe cartilage degeneration and greater intervertebral rotation. **A** Representative 3D reconstruction of a scoliotic spine by EOS. Selected facet joint regions are highlighted in blue (above or below) and yellow (apex). **B** Relative M-CSF gene expression levels above and below the apex compared to the apex (patients *n*=19, facet joints above *n*=28, apex *n*=19, below *n*=20).Data was analyzed using Kruskal-Wallis test. **C** Cartilage morphological grading of the selected levels (patients *n*=19, facet joints above *n*=30, apex *n*=19, below *n*=23). Data was analyzed using Kruskal-Wallis test. Figure **D**. Degree of intervertebral rotation at the selected levels (patients *n*=18, facet joints above *n*=27, apex *n*=18, below*n*=19). Data was analyzed using ANOVA with Dunnett's T3 multiple comparisons test. **E** Spearman correlation of MCSF gene expression, degeneration grade, intervertebral angle **F**. *P*-value of the Spearman correlations.Significance defined by **P*< .05, ***P*< .01, ****P*< .001, *****P*<0.0001. Figure layout designed using the BioRender.com platform

The interplay between cartilage and bone, particularly through subchondral pores, has been implicated in adult knee and hip OA [17, 21, 29], however, the mechanism remains unexplored in facet joints of young patients with AIS. Our study indicates that the TLR-M-CSF axis is strongly implicated in facet joint chondrocytes of AIS patients and as such may drive osteoclast proliferation and maturation, resulting in increased bone turnover.

TLR activation, triggered by damage-associated molecular patterns (DAMPs), has been linked to OA pathogenesis in the knee, hip, and facet joints, where it is proposed to induce the production of pro-inflammatory mediators and proteases that drive tissue degradation [24, 30]. The current study discovered 1,426 DEGs significantly upregulated in AIS facet joint chondrocytes. Many of these genes were enriched in the TLR2 and 4 pathways along with chemokine/cytokine-mediated pathways. TLR2 was identified as a key hub gene within the highest-ranked PPI network cluster, highlighting its crucial role in cartilage degeneration in AIS. The results reinforce findings from our earlier studies [24] Those studies identified endogenous TLR agonists (alarmins) and determined that TLR2 gene expression was elevated in AIS facet joint cartilage and although TLR4 was not elevated it was robustly expressed and responsive to trigger [24].

Osteoarthritic chondrocytes produce a spectrum of pro-inflammatory mediators with known direct and indirect functions in osteoclasts [22, 23, 31, 32]. In line with previous studies, the current RNAseq analysis indicated higher levels of bone regulatory cytokines/chemokines in AIS chondrocytes. This finding was further supported by qPCR and ELISA confirming the upregulation of RANKL, M-CSF, GM-CSF, IL-1, IL-6, IL-8, IL-17, CXCL-1, CXCL-10, and TNFα. Importantly, RANKL

and M-CSF are crucial factors for osteoclastogensis [33]. Although it has previously been shown, by us and others, that IL-1, IL-6, and IL-8 are downstream targets of TLR activation [24, 30], the link between TLR activation and the additional factors influencing bone regulation was previously unexplored in AIS. We found that pro-osteoclastogenic genes were more robustly upregulated than anti- osteoclastogenic genes following TLR activation. This suggests a shift in the secretory profile towards pro-osteoclastogenesis, a phenomenon similarly observed in bone loss linked to other inflammatory conditions [34]. We confirmed the protein levels of 14 factors; all except one showed a significantly increased protein concentration following TLR activation, consistent with gene expression results. TLRs display a distinct expression pattern in OA cartilage based on the joint type [35]. According to Bisson et al., TLR2 is expressed at higher levels than TLR1, TLR4, and TLR6 in AIS facet joints when compared to non-scoliotic facet joints [24]. Although expressed at different levels, there was no significant difference in the induction of bone-regulating cytokines following TLR2 and TLR4 activation with specific agonists. Despite their different ligand specificities and dimerization patterns, both TLR2 and TLR4 trigger similar downstream signalling pathways that lead to NF-κB activation and may explain the similarity in the secretory profile following activation [36].

M-CSF is an essential cytokine promoting differentiation and survival of monocytes/macrophages. It is usually secreted by immune cells including neutrophils and macrophages in response to TLR-driven microbicidal activity. Our study is the first to demonstrate its induction in articular chondrocytes following TLR2 or TLR4 activation [37]. Some studies suggest that increased M-CSF expression in OA cartilage may stimulate proteoglycan production in a potential attempt to protect the cartilage [38–41]. However, M-CSF is a multifunctional cytokine and a key factor for the proliferation and survival of osteoclast precursors. The increased expression of M-CSF in AIS facet joint cartilage could also allow M-CSF diffusion through subchondral pores, promoting osteoclast proliferation and maturation [42]. Here, we demonstrated that conditioned media from AIS chondrocytes enhanced osteoclast precursor proliferation. The effect was intensified when the chondrocytes were preactivated with TLR2 or TLR4 agonists [42–44] and multinucleated osteoclasts were significantly increased after exposure to AIS-CCM. This effect was further amplified when the chondrocytes were preactivated with TLR2 or TLR4 agonists and may be a direct result of the higher M-CSF concentration in CCM from TLR-activated AIS chondrocytes.

We and others have previously shown that cartilage and subchondral bone deterioration varies across the scoliotic spine [8, 14, 45, 46]. While the TLR-MCSF axis appears to boost osteoclast proliferation and differentiation in vitro, our current study does not address osteoclast activity in intact facet joints across the scoliotic spine, representing a limitation of our research. Technical challenges of inconsistent TRAP enzyme activity affected by fixation and decalcification make osteoclast quantification by histology difficult in intact human facet joints. We, therefore, resorted to evaluating M-CSF gene expression as an indirect measure of osteoclast activity. The levels were selected based on the study by Bisson et al., which showed more severe OA and greater axial rotation 2–4 levels above and below the apex [15]. We found a consistent and positive correlation between OA score and degree of intervertebral rotation in this cohort of patients. MCSF expression levels were not correlated with sagittal or coronal angles. There was also no significant correlation between baseline M-CSF expression and Cobb angle in this cohort (Supplementary data 6). Collectively, the gene expression pattern of M-CSF may suggest a higher bone turnover rate in facet joints above the apex where OA score and intervertebral rotation is the greatest.

There are no widely accepted animal models that spontaneously develop scoliosis. While some transgenic mouse models develop scoliosis, they do so inconsistently, and the modified gene is typically only found in a small fraction (less than 10%) of AIS patients. Additionally, induced scoliosis models—such as those based on amputation or forced upright posture in mice, primarily affect the lumbar region, they are ethically questionable and may not fully recapitulate the characteristics of human AIS. In human patients, we can only analyze the facet joints when removed to allow for curve correction. It is, therefore, not possible to conduct time-point studies in humans and without an animal model, it is challenging to determine whether OA precedes intervertebral rotation or arises as a consequence. According to the "vicious cycle" theory proposed by Stokes, asymmetrical forces lead to asymmetrical growth and progressive deformity, which in turn amplify the forces over time and accelerate curve progression. These forces can contribute to OA and affect the entire joint, potentially influencing rotation. As rotation increases and deformity worsens, OA may also progress, further reinforcing this mutual relationship.

The relationship between cartilage and bone is inseparable in the progression of OA. The TLR-M-CSF axis may function as a double-edged sword and provide a protective role in the early stage of facet joint OA. In later stages when the protective mechanism is insufficient to prevent OA progression M-CSF may diffuse through the subchondral pores and disrupt bone homeostasis. Such disruptions and continued adverse asymmetrical loading

may exacerbate OA severity [14, 47], and drive growth modulation with modifications of facet joint size and shape [8, 15, 45]. Together, it may further decrease spinal stability and increase vertebral rotation, tilting, and concave lordosis, thus fueling the vicious cycle of curve progression [48]. Understanding the molecular interplay between cartilage and bone could indicate potential therapeutic targets to reduce AIS progression. One potential target is TLR inhibitors that may decrease the inflammatory and degenerative environment in AIS cartilage, thereby reducing the negative impact on the subchondral bone.

Conclusion

Secreted factors from AIS chondrocytes enhance osteoclast proliferation and maturation and may result in increased bone turnover. M-CSF expression was strongly correlated with increased OA severity and a greater degree of intervertebral axial rotation in facet joints above and below the apex. Together, our findings suggest that the TLR-M-CSF axis is implicated in osteoclastogenesis, resulting in increased bone turnover and may contribute to curve progression in AIS patients.

Abbreviations

AIS	Adolescent Idiopathic Scoliosis
CCLs	Chemokine (C–C motif) Ligands
CCM	Chondrocyte Conditioned Media
CXCLs	Chemokine (C-X-C motif) Ligands
DEG	Differentially Expressed Gene
GSEA	Gene Set Enrichment Analysis
GM-CSF	Granulocyte–Macrophage Colony-Stimulating Factor
GO	Gene Ontology
IFN-γ	Interferon-Gamma
ILs	Interleukins
M-CSF	Macrophage Colony-Stimulating Factor
MNC	Maximum Neighborhood Component
MnOC	Multi-nuclear Osteoclast
NSC	Non-Scoliotic Control
OA	Osteoarthritis
OPG	Osteoprotegerin
PPI-network	Protein–Protein Interaction Network
RANKL	Receptor Activator of Nuclear Factor Kappa-B Ligand
RNAseq	RNA Sequencing
TLR2	Toll-Like Receptor 2
TLR2A	Toll-Like Receptor 2 Agonist
TLR4	Toll-Like Receptor 4
TLR4A	Toll-Like Receptor 4 Agonist
TNF-α	Tumor Necrosis Factor-Alpha
TRAP	Tartrate-Resistant Acid Phosphatase
UCM	Unconditioned Media

Supplementary Information

The online version contains supplementary material available at https://doi.org/10.1186/s13075-025-03535-6.

Supplementary Material 1: Figure 1A, MCODE analysis showing the top 16 clusters, each detailed with nodes and edges. Figure 1B PCA of RNAseq data reveals a distinct separation between AIS and NSC samples. Figure 1C illustrates the GO analysis (KEGG pathway) of the 5 first clusters. Dot size indicates the number of enriched genes, while dot colour denotes statistical significance (FDR). Figure layout designed using the BioRender.com platform

Supplementary Material 2: Figure 2, Baseline gene expression profile for TLRs in facet joint chondrocytes from scoliotic ($n=11–13$) and non-scoliotic ($n=16$) subjects. Data was analyzed using a two-tailed Mann–Whitney U test. Figure layout designed using the BioRender.com platform.

Supplementary Material 3: Figure 3, With the known importance of glucose in cell proliferation and the different glucose concentrations in the chondrocyte culture medium DMEM (4.5g/L) and osteoclast culture medium αMEM (1g/L), we used the AlamarBlue assays to determine if combining DMEM and αMEM 1:4 would inherently affect osteoclast precursor proliferation . We found no significant difference in metabolic activity in the evaluated conditions, suggesting that a slightly higher glucose concentration was not a confounding factor in our experimental conditions ($n=5$). Figure layout designed using the BioRender.com platform.

Supplementary Material 4: Figure 4, TRAP staining to determine osteoclast differentiation following exposure to CCM at varying concentrations ranging from 1–50%. Figure layout designed using the BioRender.com platform

Supplementary Material 5: Figure 5, Comparison of EOS 3D data between the two evaluators. A. Scatter plots showed a strong correlation between the data points from the evaluators. B. Bland–Altman plots depict the difference of each data point from the mean average, with very few outliers, indicating consistency between the evaluators. C. Histograms show the distribution of all data points and the overlap between the two evaluators and illustrate similar data spread and agreement across the planes

Supplementary Material 6: Figure 6, Scatter plots showing the relationship between MCSF levels and Cobb angle. The x-axis represents MCSF levels, while the y-axis represents Cobb angle measurements. A linear regression line is fitted to the data, with regression analysis presented in the adjacent table, including the equation of the fitted line, R-squared value, and statistical significance. There is no significant correlation between MCSF levels—of pooled samples or selected levels—and the Cobb angle

Acknowledgements

The authors kindly acknowledge the help from staff and surgeons at the Shriner's Hospital for Children.

Declaration of generative AI and AI-assisted technologies in the writing process

The authors used Grammarly to check spelling and to revise the sentences. The content was then reviewed and edited as needed, and the authors assume full responsibility for the content of the publication.

Authors' contributions

KS and LH were responsible for the conception and design of the study. KS and DB acquired the facet joint data. JB and CC reconstructed spinal models for the intervertebral angle data. KS performed the analysis and interpretation of the data and drafted the initial manuscript. NS, KU, and JO, as orthopedic surgeons, were responsible for performing AIS surgeries and harvesting tissues from organ donors. KT and SK were responsible for sacrificing mice to isolate bone marrow monocytes. All author participated in revising and submitting the final manuscript.

Funding

This study was funded by the Shriner's Hospital for Children (72002-CAN-23) and the Canadian Institutes of Health Research (PJT-183867). KS received a studentship from Fonds de recherche du Québec Santé (FRQS).

Data availability

No datasets were generated or analysed during the current study.

Declarations

Ethics approval and consent to participate
The study was approved by the McGill University institutional review board in Montreal, Canada (IRB # Tissue Biobank 2019–4896 and A03-M10-23A). Written informed consent was received before participation in the study.

Consent for publication
The authors confirm that all participants involved in the study have provided written informed consent for publication of the results and any accompanying data/images in this manuscript.

Competing interests
The authors declare no competing interests.

Author details
[1]Shriners Hospital for Children, Montreal, QC, Canada. [2]Department of Surgery, Orthopaedic Research Laboratory, Mcgill University, Montreal, QC, Canada. [3]Mcgill University Health Centre, Montreal, QC, Canada. [4]University of Alberta, Edmonton, AB, Canada.

Received: 3 December 2024 Accepted: 12 March 2025
Published online: 31 March 2025

References

1. Cheng JC, Castelein RM, Chu WC, Danielsson AJ, Dobbs MB, Grivas TB, et al. Adolescent idiopathic scoliosis. Nat Rev Dis Primers. 2015;1:15030.
2. Wong C. Mechanism of right thoracic adolescent idiopathic scoliosis at risk for progression; a unifying pathway of development by normal growth and imbalance. Scoliosis. 2015;10:2.
3. Smit TH. Adolescent idiopathic scoliosis: The mechanobiology of differential growth. Jor Spine. 2020;3: e1115.
4. Marya S, Tambe AD, Millner PA, Tsirikos AI. Adolescent idiopathic scoliosis : a review of aetiological theories of a multifactorial disease. bone Jt J. 2022;104-B:915–21.
5. Burwell RG, Clark EM, Dangerfield PH, Moulton A. Adolescent idiopathic scoliosis (AIS): a multifactorial cascade concept for pathogenesis and embryonic origin. Scoliosis Spinal Disord. 2016;11:8.
6. Burwell RG, Dangerfield PH, Moulton A, Grivas TB. Adolescent idiopathic scoliosis (AIS), environment, exposome and epigenetics: a molecular perspective of postnatal normal spinal growth and the etiopathogenesis of AIS with consideration of a network approach and possible implications for medical therapy. Scoliosis. 2011;6:26–26.
7. Hawary RE, Zaaroor-Regev D, Floman Y, Lonner BS, Alkhalife YI, Betz RR. Brace treatment in adolescent idiopathic scoliosis: risk factors for failure—a literature review. Spine J. 2019;19:1917–25.
8. Schlager B, Krump F, Boettinger J, Niemeyer F, Ruf M, Kleiner S, et al. Characteristic morphological patterns within adolescent idiopathic scoliosis may be explained by mechanical loading. Eur Spine J. 2018;27:2184–91.
9. Jaumard NV, Welch WC, Winkelstein BA. Spinal Facet Joint Biomechanics and Mechanotransduction in Normal, Injury and Degenerative Conditions. J Biomechanical Eng. 2011;133: 071010.
10. Inoue N, Orías AAE, Segami K, An and HS. Chapter 10: Function and Dysfunction of the Facet Joint. In: Boden SD, MD, editors. Lumbar Spine Textbook. 2002. p. 1254.
11. Kelly A, Younus A, Lekgwara P. Adult degenerative scoliosis – A literature review. Interdiscip Neurosurg. 2020;20: 100661.
12. Kojima S, Ikemoto T, Arai Y-C, Hirasawa A, Deie M, Takahashi N. Associations between Degenerative Lumbar Scoliosis Structures and Pain Distribution in Adults with Chronic Low Back Pain. Healthcare. 2023;11:2357.
13. Netzer C, Distel P, Wolfram U, Deyhle H, Jost GF, Schären S, et al. Comparative Analysis of Bone Structural Parameters Reveals Subchondral Cortical Plate Resorption and Increased Trabecular Bone Remodeling in Human Facet Joint Osteoarthritis. Int J Mol Sci. 2018;19:845.
14. Bisson DG, Lama P, Abduljabbar F, Rosenzweig DH, Saran N, Ouellet JA, et al. Facet joint degeneration in adolescent idiopathic scoliosis. Jor Spine. 2018;1: e1016.
15. Bisson DG, Sheng K, Kocabas S, Ocay DD, Ferland CE, Saran N, et al. Axial rotation and pain are associated with facet joint osteoarthritis in adolescent idiopathic scoliosis. Osteoarthr Cartil. 2023;31:1101–10.
16. Clarke J. Bone stresses out cartilage in OA. Nat Rev Rheumatol. 2021;17:250–250.
17. Burr DB, Gallant MA. Bone remodelling in osteoarthritis. Nat Rev Rheumatol. 2012;8:665–73.
18. Li G, Yin J, Gao J, Cheng TS, Pavlos NJ, Zhang C, et al. Subchondral bone in osteoarthritis: insight into risk factors and microstructural changes. Arthritis Res Ther. 2013;15:223.
19. Mansell JP, Collins C, Bailey AJ. Bone, not cartilage, should be the major focus in osteoarthritis. Nat Clin Pr Rheumatol. 2007;3:306–7.
20. Pan J, Wang B, Li W, Zhou X, Scherr T, Yang Y, et al. Elevated cross-talk between subchondral bone and cartilage in osteoarthritic joints. Bone. 2012;51:212–7.
21. Hu W, Chen Y, Dou C, Dong S. Microenvironment in subchondral bone: predominant regulator for the treatment of osteoarthritis. Ann Rheum Dis. 2021;80:413–22.
22. Brylka LJ, Schinke T. Chemokines in Physiological and Pathological Bone Remodeling. Front Immunol. 2019;10:2182.
23. Souza PPC, Lerner UH. The role of cytokines in inflammatory bone loss. Immunol Invest. 2013;42:555–622.
24. Bisson DG, Sheng K, Kocabas S, Krock E, Teles A, Saran N, et al. Toll-like receptor involvement in adolescent scoliotic facet joint degeneration. J Cell Mol Med. 2020;24:11355–65.
25. Li J, Muehleman C, Abe Y, Masuda K. Prevalence of facet joint degeneration in association with intervertebral joint degeneration in a sample of organ donors. J Orthopaed Res. 2011;29:1267–74.
26. Armstrong S, Pereverzev A, Dixon SJ, Sims SM. Activation of P2X7 receptors causes isoform-specific translocation of protein kinase C in osteoclasts. J Cell Sci. 2008;122:136–44.
27. Bisson DG. Investigating facet joint osteoarthritis in the context of adolescent idiopathic scoliosis. Thesis. 2018;1: e1016.
28. Li M, Xie W, He M, Yu D, Xu D, Xiao W, et al. Characterization of the Subchondral Bone and Pain Behavior Changes in a Novel Bipedal Standing Mouse Model of Facet Joint Osteoarthritis. Biomed Res Int. 2020;2020:8861347.
29. Tat SK, Lajeunesse D, Pelletier J-P, Martel-Pelletier J. Targeting subchondral bone for treating osteoarthritis: what is the evidence? Best Pract Res Clin Rheumatology. 2010;24:51–70.
30. Barreto G, Manninen M, Eklund KK. Osteoarthritis and Toll-Like Receptors: When Innate Immunity Meets Chondrocyte Apoptosis. Biology. 2020;9:65.
31. Amarasekara DS, Yun H, Kim S, Lee N, Kim H, Rho J. Regulation of Osteoclast Differentiation by Cytokine Networks. Immune Netw. 2018;18: e8.
32. Kitaura H, Kimura K, Ishida M, Sugisawa H, Kohara H, Yoshimatsu M, et al. Effect of Cytokines on Osteoclast Formation and Bone Resorption during Mechanical Force Loading of the Periodontal Membrane. Sci World J. 2014;2014: 617032.
33. Kim JH, Kim N. Signaling Pathways in Osteoclast Differentiation. Chonnam Medical J. 2016;52:12–7.
34. Hardy R, Cooper MS. Bone loss in inflammatory disorders. J Endocrinol. 2009;201:309–20.
35. Barreto G, Sandelin J, Salem A, Nordström DC, Waris E. Toll-like receptors and their soluble forms differ in the knee and thumb basal osteoarthritic joints. Acta Orthop. 2017;88:1–8.
36. Shavit ZB. Synergy in Toll-Like Receptors (TLRs) . J Cell Signal. 2017;2:1–2.
37. Hübel K, Dale DC, Liles WC. Therapeutic Use of Cytokines to Modulate Phagocyte Function for the Treatment of Infectious Diseases: Current Status of Granulocyte Colony-Stimulating Factor, Granulocyte-Macrophage Colony-Stimulating Factor, Macrophage Colony-Stimulating Factor, and Interferon-γ. J Infect Dis. 2002;185:1490–501.
38. Campbell IK, Novak U, Cebon J, Layton JE, Hamilton JA. Human articular cartilage and chondrocytes produce hemopoietic colony-stimulating factors in culture in response to IL-1. J Immunol (Baltim, Md : 1950). 1991;147:1238–46.
39. Nakao K, Kubota S, Doi H, Eguchi T, Oka M, Fujisawa T, et al. Collaborative action of M-CSF and CTGF/CCN2 in articular chondrocytes: Possible regenerative roles in articular cartilage metabolism. Bone. 2005;36:884–92.

40. Campbell IK, Ianches G, Hamilton JA. Production of macrophage colony-stimulating factor (M-CSF) by human articular cartilage and chondrocytes. Modulation by interleukin-1 and tumor necrosis factor α. Biochim Biophys Acta (BBA) - Mol Basis Dis. 1993;1182:57–63.
41. Truong M-D, Choi BH, Kim YJ, Kim MS, Min B-H. Granulocyte macrophage – colony stimulating factor (GM-CSF) significantly enhances articular cartilage repair potential by microfracture. Osteoarthr Cartil. 2017;25:1345–52.
42. Rahman MM, Takeshita S, Matsuoka K, Kaneko K, Naoe Y, Sakaue-Sawano A, et al. Proliferation-coupled osteoclast differentiation by RANKL: Cell density as a determinant of osteoclast formation. Bone. 2015;81:392–9.
43. Remmers SJA, van der Heijden FC, Ito K, Hofmann S. The effects of seeding density and osteoclastic supplement concentration on osteoclastic differentiation and resorption. Bone Reports. 2022;18: 101651.
44. Quinn JMW, Gillespie MT. Modulation of osteoclast formation. Biochem Biophys Res Commun. 2005;328:739–45.
45. Yahara Y, Seki S, Makino H, Futakawa H, Kamei K, Kawaguchi Y. Asymmetric Load Transmission Induces Facet Joint Subchondral Sclerosis and Hypertrophy in Patients with Idiopathic Adolescent Scoliosis: Evaluation Using Finite Element Model and Surgical Specimen. JBMR Plus. 2023;7: e10812.
46. Zhang H, Wang L, Liu S, Li J, Xiao L, Yang G. Adiponectin regulates bone mass in AIS osteopenia via RANKL/OPG and IL6 pathway. J Transl Med. 2019;17:64.
47. O'Leary SA, Paschos NK, Link JM, Klineberg EO, Hu JC, Athanasiou KA. Facet Joints of the Spine: Structure-Function Relationships, Problems and Treatments, and the Potential for Regeneration. Annu Rev Biomed Eng. 2018;20:1–26.
48. Burwell RG. Etiology of Adolescent Idiopathic Scoliosis: Current Trends and Relevance to New Treatment Approaches [Internet]. Hanley & Belfus, Incorporated; 2000. Available from: https://books.google.ca/books?id=htPkAAAACAAJ.

Publisher's Note